The Astrophysical Journal, 595:L57–L61, 2003 September 20
© 2003. The American Astronomical Society. All rights reserved. Printed in U.S.A.

A THREE-DIMENSIONAL MODEL OF THE SOLAR WIND INCORPORATING SOLAR MAGNETOGRAM OBSERVATIONS

I. I. Roussev,[1] T. I. Gombosi,[1] I. V. Sokolov,[1] M. Velli,[2,3] W. Manchester IV,[1]
D. L. DeZeeuw,[1] P. Liewer,[2] G. Tóth,[1,4] and J. Luhmann[5]
Received 2003 July 3; accepted 2003 August 4; published 2003 August 26

ABSTRACT

We present a new compressible MHD model for simulating the three-dimensional structure of the solar wind under steady state conditions. The initial potential magnetic field is reconstructed throughout the computational volume using the source surface method, in which the necessary boundary conditions for the field are provided by solar magnetogram data. The solar wind in our simulations is powered by the energy interchange between the plasma and large-scale MHD turbulence, assuming that the additional energy is stored in the "turbulent" internal degrees of freedom. In order to reproduce the observed bimodal structure of the solar wind, the thermodynamic quantities for the initial state are varied with the heliographic latitude and longitude depending on the strength of the radial magnetic field.

Subject headings: interplanetary medium — methods: numerical — MHD — solar wind — Sun: evolution — Sun: magnetic fields

On-line material: mpeg animation

1. INTRODUCTION

The global structure of the solar wind results from the complex interaction between the expanding coronal plasma, magnetic fields, solar rotation, and interplanetary turbulence. The observed dichotomy between a fast solar wind and a slow solar wind (Phillips et al. 1995; Goldstein et al. 1996) results from the topological structure of the solar magnetic fields that are divided into open field and closed field regions by the boundaries of helmet-like streamers. Unlike open field regions (associated with coronal holes), magnetic fields in helmet streamers are bipolar, and their strength is large enough to prevent the bulk expansion of coronal plasma.

The simulation runs presented in this Letter are designed to reproduce the global structure of the heliosphere under realistic conditions. The initial magnetic field at the solar surface is taken from synoptic maps, and the field is reconstructed into the simulation volume through a potential field extrapolation (Altschuler et al. 1977). The MHD solution is allowed to evolve from this initial configuration to a fully self-consistent, nonpotential solution.

Our model was inspired by a multitude of previous numerical efforts pioneered by Pneuman & Kopp (1971), who first studied the steady, axisymmetric expansion of coronal plasma from a sphere with an embedded dipolar magnetic field. Similar magnetic configurations were used in the majority of later studies in two dimensions (see Wang et al. 1998 and Suess et al. 1999) and three dimensions (see Usmanov 1993 and Groth et al. 2000), in order to model the solar wind conditions representing the heliosphere at solar minimum. Most studies have successfully reproduced the global structure of the outer solar corona, but the bimodality of the solar wind could not be modeled in a quantitative manner without adding proper empirical sources to power the wind in open field regions. The incorporation of Alfvén waves in the momentum balance and energetics of the solar wind was studied extensively in one-dimensional magnetohydrodynamics (see Holzer, Flå, & Leer 1983 and McKenzie, Axford, & Banaszkiewicz 1997). The effect of an Alfvén wave flux on the flow properties of the solar wind, in a WKB approximation, was recently studied in two dimensions by Usmanov et al. (2000). These results are in good agreement with the *Ulysses* data normalized to 1 AU. The dissipation of an Alfvén wave spectrum at the ion-cyclotron frequency might additionally lead to preferential heating of the ions in open field regions (Axford & McKenzie 1992).

We are still taking the first steps in modeling the global structure of the heliosphere for realistic conditions derived from solar magnetogram data (Linker et al. 1999; Riley, Linker, & Mikić 2001). In this Letter, we present further attempts in this direction, which employ a fully three-dimensional and compressible MHD in our simulations. We allow for the polytropic index to change with radial distance from the Sun (Wu et al. 1999), but in our model, a form of the total energy is conserved.

2. MODEL

In order to simulate the large-scale structure of the corona properly, one has to consider the solar plasma as a gas with a polytropic index γ close to unity (Steinolfson & Hundhausen 1988), say $\gamma \approx 1.1$, close to the Sun. Near the Earth, however, observations indicate that the polytropic index of the solar wind plasma has a value of $\gamma_0 \approx 1.5$ (Phillips et al. 1995; Totten, Freeman, & Arya 1995). This could be interpreted as the ratio of specific heats for a gas of particles with $n \approx 4$ degrees of freedom since, in general, $\gamma_0 = (n + 2)/n$. For a fully ionized plasma, such as the solar wind, there are almost no species with standard internal degrees of freedom such as those arising from molecule vibrations, rotations, and bound-bound and bound-free electron transitions in atoms/ions. However, especially close to the Sun, a significant amount of energy is stored in waves and turbulent fluctuations. We therefore adopt a mod-

[1] Center for Space Environment Modeling, University of Michigan at Ann Arbor, 2455 Hayward Street, Ann Arbor, MI 48109-2143; iroussev@umich.edu.
[2] Jet Propulsion Laboratory, California Institute of Technology, 4800 Oak Grove Drive, Pasadena, CA 91109.
[3] Department of Astronomy and Space Science, University of Florence, Largo Enrico Fermi 5, Florence I-50125, Italy.
[4] Department of Atomic Physics, Loránd Eötvös University, Budapest H-1117, Hungary.
[5] Space Sciences Laboratory, University of California at Berkeley, Grizzly Peak at Centennial Drive, Berkeley, CA 94720-3411.

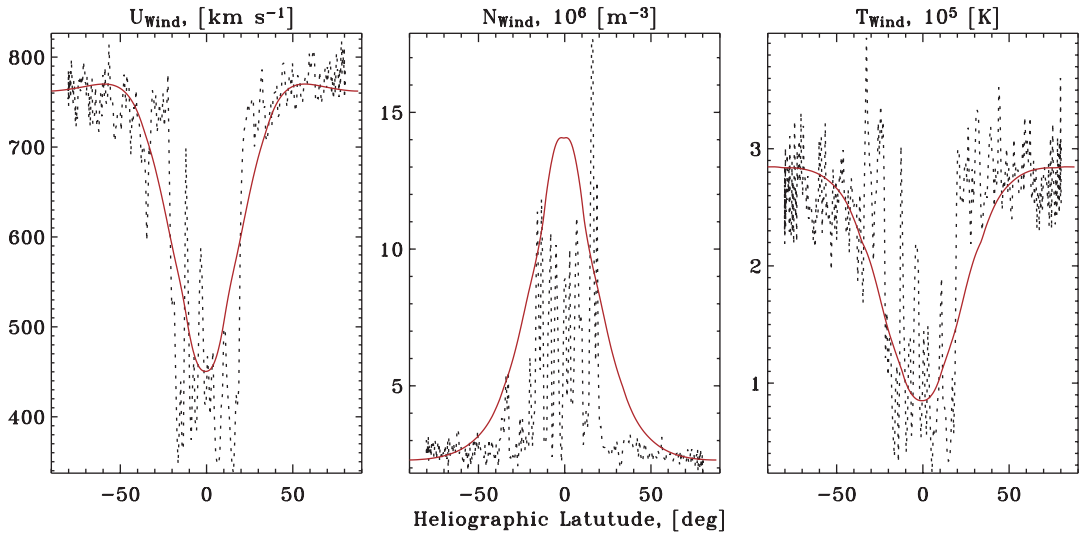

FIG. 1.—Comparison between *Ulysses* data normalized to 1 AU (*dotted curves in black*) and simulation results for a nontilted, rotating magnetic dipole (*solid curves in red*).

eling approach in which low values of γ are associated with such "turbulent" internal degrees of freedom, in a way analogous to the work of Zeldovich & Raizer (2002) in partially ionized plasmas.

Within some temperature intervals, the ratio of specific heats for partially ionized plasmas is very close to unity, or, equivalently, the specific heat $(\gamma - 1)^{-1} = n/2$ is very large precisely because energy can be stored in a form of the ionization potential of decoupled electrons, and it can be deposited in the course of plasma recombination as these electrons rejoin the ions. The contribution of the specific heat due to internal degrees of freedom is $(\gamma - 1)^{-1} - (\gamma_0 - 1)^{-1} = (n - 4)/2$, and the additional internal energy may be expressed as $E_{st} = [P(n - 4)/2](T_{st}/T)$. Here P is the plasma pressure, and T_{st} is the temperature in the internal degrees of freedom, which generally differs from the kinetic plasma temperature, T. The full energy balance in this case is given by one more equation for E_{st} describing the energy exchange between the classical and internal degrees of freedom in terms of temperature relaxation, namely,

$$(\text{energy eq. with } \gamma = \gamma_0) = \frac{E_{st} - P(n-4)/2}{\tau_{rel}}, \qquad (1)$$

$$\frac{\partial E_{st}}{\partial t} + \nabla \cdot (\boldsymbol{U} E_{st}) = -\frac{E_{st} - P(n-4)/2}{\tau_{rel}}, \qquad (2)$$

where τ_{rel} is the relaxation time. If this time tends to infinity, the stored and classical internal energies are conserved independently, while in general only the total is conserved.

Following this approach, we assume that the energy of turbulent motions near the Sun can also be treated as the extra energy stored in the plasma, in a manner analogous to equations (1) and (2). Note that phenomenological models of turbulence based on "hydrodynamical" equations for the turbulent energy

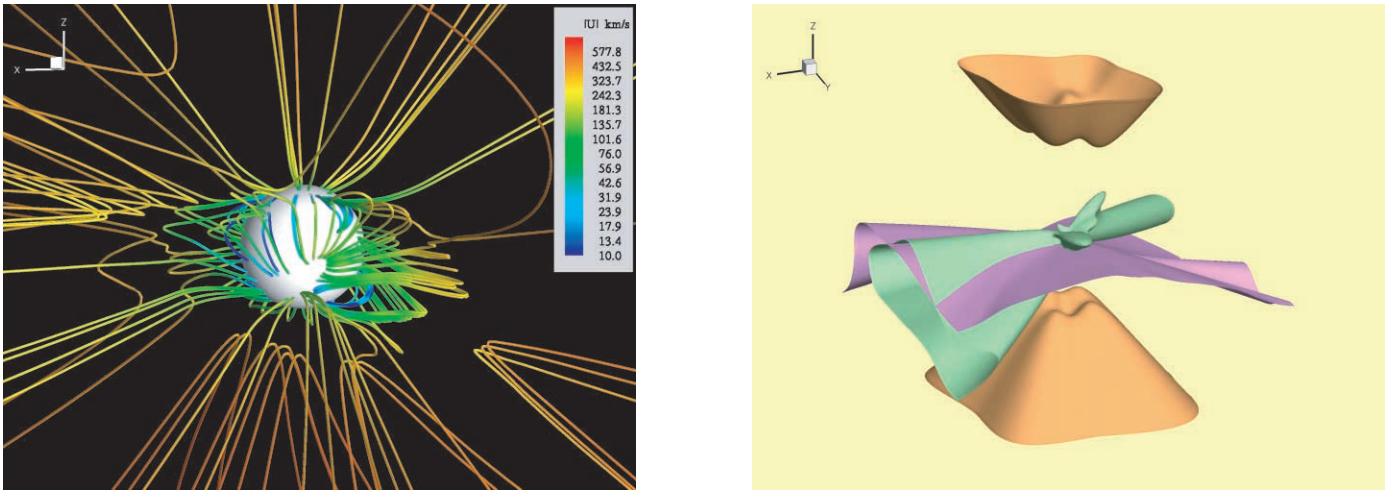

FIG. 2.—*Left:* Three-dimensional view of the magnetic field geometry near the Sun. The solid lines are magnetic field lines, where the false-color code visualizes the wind speed in kilometers per second. *Right:* Three-dimensional view far from the Sun showing isosurfaces of a wind speed of 470 km s^{-1} (*shaded in green*); a wind speed of 760 km s^{-1} (*orange*); and a zero radial magnetic field (*purple*). This figure is also available as an mpeg animation in the electronic edition of the *Astrophysical Journal*.

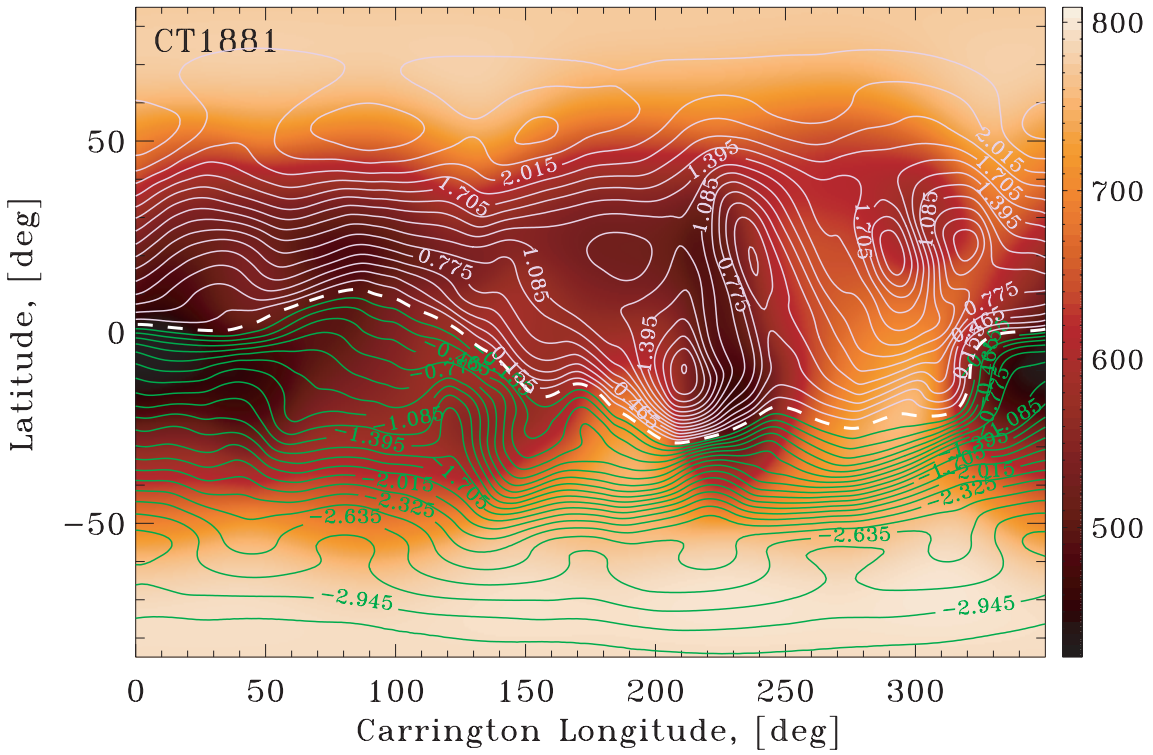

FIG. 3.—Mercator map projection of the steady state wind speed in kilometers per second (*background image*) and the radial magnetic field (*contours*) at 1 AU. The position of the current sheet is shown as the dashed contour in white. The magnetic field strength is given in units of nanotesla.

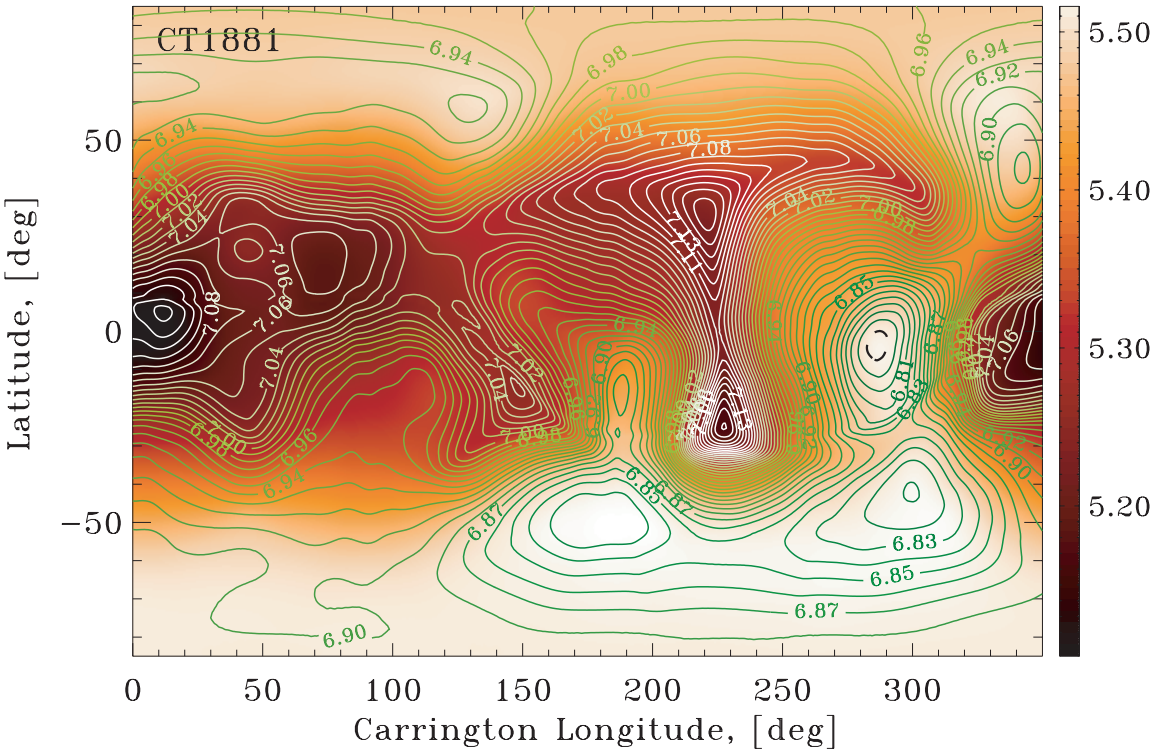

FIG. 4.—Mercator map projection of the steady state wind temperature in kelvins (*image*) and the number density in units of m^{-3} (*contours*) at 1 AU. Both quantities are shown in a logarithmic scale. The dashed contour line in black marks the minimum value of number density.

density with some "equation of state" for the latter are widely used in applied physics (see Saurel, Chinnayya, & Renaud 2003 and the references therein). The role of the energy interchange depends on the relation between the relaxation time, $\tau_{\rm rel}$, and the characteristic hydrodynamical time, $\tau_{\rm hyd}$. If $\tau_{\rm hyd} \gg \tau_{\rm rel}$, then $E_{\rm st} \approx P(n-4)/2$, and the resulting energy equation (the sum of eqs. [1] and [2]) is for $\gamma = (n+2)/n$. In the opposite limit, $\tau_{\rm hyd} \ll \tau_{\rm rel}$, equation (1) is valid for $\gamma = \gamma_0$, and equation (2) is not needed. In our numerical model, we choose $\tau_{\rm rel}$ to be as small as possible (of the order of the time step). We further assume that the internal degrees of freedom depend on the kinetic plasma temperature as $n(T) = n_0 + n_1 T/T_0$, where we choose $n_0 = 4$ and $n_1 = 9$ following the discussion above. Here T_0 is some reference value of temperature at the Sun that will be defined later. Thus, we employ the full energy equation in our computations with a polytropic index $\gamma = [n(T) + 2]/n(T)$, which is now a function of temperature describing the additional energy density associated with turbulent motions. We note that this technique is an empirical one inspired by the "hidden internal" degrees of freedom. This is only a model we are using to bridge from a polytrope, which is nearly isothermal, to a fully fledged energy equation with wave coupling and heating.

In the static initial state, the plasma temperature as a function of radial distance from the Sun, R, can be obtained from the differential equation of state, namely, $dp = \{\gamma(T)/[\gamma(T) - 1]\}\,\rho\, dT$, and the equation for hydrostatic equilibrium in the absence of magnetic field, i.e., $dp = GM_\odot \rho d(1/R)$. (We work in units where the universal gas constant equals the mean molecular weight.) As a result of simple integration from $R_\odot$ to R, we obtain the following quadratic equation for $u(R) = T(R)/T_0$:

$$u^2 + \frac{4}{n_1}\left(1 + \frac{n_0}{2}\right)u - \frac{4}{n_1}\left(1 + \frac{n_0}{2} + \frac{n_1}{4}\right)\frac{R_\odot}{R} = 0. \qquad (3)$$

Here the reference temperature T_0 is chosen such that the asymptotic behavior of $u(R)$ at large distances is $\sim 1/R$, so that $u \to 0$ as $R \to \infty$. Furthermore, this choice is consistent with solar wind observations showing that $\rho \sim 1/R^2$ and $T \sim 1/R$ for $\gamma \approx 1.5$. The explicit choice for T_0 reads $T_0 = GM_\odot/[R_\odot(1 + n_0/2 + n_1/4)]$. Once the temperature is derived from equation (3), the plasma pressure can be obtained from $d\ln(p/p_0) = \{\gamma(T)/[\gamma(T) - 1]\} d\ln(T/T_0) = [1 + n_0/2 + n_1 u/2] d\ln u$, following a direct integration. (Here p_0 is the reference value for pressure at $R_\odot$, where $T = T_0$.) As a result,

$$p = p_0 u^{(1+n_0/2)} \exp\left[-\frac{n_1(1-u)}{2}\right]. \qquad (4)$$

From the equation of state, the mass density is $\rho = \rho_0(p/p_0)/u$, where $\rho_0 = p_0/T_0 = 1$ (in units of 8.36×10^{-14} kg m^{-3}). For $n_0 = 4$ and $n_1 = 9$, the value of T_0 becomes 4.402×10^6 K, and $u(R) = T(R)/T_0$ ranges from 1 at $R = R_\odot$ to 8.053×10^{-3} at $R = 1$ AU. Accordingly, $\gamma(R)$ ranges from 1.154 at the solar surface to 1.491 at 1 AU.

In order to reproduce the observed bimodal structure of the solar wind, we impose a temperature variation on the solar surface depending on the strength of the radial magnetic field. This is chosen as $T[R_\odot, B_R(\theta,\phi)] = T_0\Lambda[B_R(\theta,\phi)] = T_0[1 + (\Lambda_t - 1)B_R(\theta,\phi)/B_0]$. Here B_R is the strength of the radial magnetic field at the surface (by absolute value), B_0 is the maximum value of B_R, and Λ_t ($\geq$1) is the ratio between the temperature where $B_R = B_0$ (magnetic poles in the case of dipole field) and that where $B_R = 0$ (magnetic equator). From this definition, $\Lambda(B_0) = \Lambda_t$ and $\Lambda(0) = 1$ are the two extremes. With this modification in place, all of the above derivations still apply, but n_1 has to be replaced by $n_1\Lambda[B_R(\theta,\phi)]$ everywhere. Since the pressure at the surface, $p[R_\odot, B_R(\theta,\phi)] = p_0(B_R)$, scales as $T_0(B_R)$, the following relation applies: $p_0(B_R)/p_0(0) = T_0(B_R)/T_0(0) = [1 + n_0/2 + n_1\Lambda(0)/4]/[1 + n_0/2 + n_1\Lambda(B_R)/4] = \Xi(B_R) \leq 1$. The mass density at the solar surface can be obtained from the equation of state, which gives $\rho_0(B_R) = \rho_0(0)\Xi(B_R)/\Lambda(B_R)$. In order to achieve good agreement between model results and solar wind data, as will be shown in § 4, it is necessary to choose $\Lambda_t = 2.10$, which gives $\Xi(0)/\Xi(B_0) = 1.47$, and so $\rho_0(0)/\rho_0(B_0) = 3.09$. Note also that for $B_R = 0$, $\gamma(R)$ ranges from 1.154 at the solar surface to 1.491 at 1 AU, while for $B_R = B_0$, these values are 1.087 and 1.474, respectively. Once derived for the initial temperature distribution, the value of γ at each point of the three-dimensional volume is maintained throughout the simulations.

3. SIMULATION SETUP

The governing equations of compressible MHD are solved in conservative form using the Block Adaptive-Tree Solar-wind Roe-type Upwind Scheme (BATS-R-US) code (Powell et al. 1999). We employ the Artificial Wind method (Sokolov et al. 2002) as an approximate Riemann solver. An explicit, two-stage time-stepping algorithm is used to advance the solution in time. The solenoidal constraint $\nabla \cdot \boldsymbol{B} = 0$ is achieved using the eight-wave scheme of Powell et al. (1999).

The simulation domain is a cube with a length of 440 $R_\odot$, and the numerical grid is nonuniform, consisting of self-similar blocks with 4^3 cells. After five levels of uniform initial refinement, we applied seven more levels of body-focused refinement in order to achieve the highest spatial resolution near the Sun. Thus, the total number of computational cells becomes 3,147,264. The smallest grid size corresponds to 0.0269 $R_\odot$, while the largest cells (near the outer boundaries) are 128 times bigger than this.

The boundary conditions describe an impenetrable and highly conducting spherical inner body, placed at $R = R_\odot = 1$, and open outer boundaries. In order to achieve line-tying of the magnetic field at the inner boundary, all velocity components are maintained at zero throughout the simulation runs, with the exception of solar rotation (which is assumed to be uniform with latitude). The pressure, turbulent energy density, $E_{\rm st}$, and mass density are fixed at the inner body. This ensures a dynamical evolution of the system toward a steady state. Floating conditions are applied to the radial and tangential components of the magnetic field. The open boundary conditions at the outer surface of the computational domain are implemented by applying a zero gradient to all physical variables.

4. "STEADY-STATE" SOLAR WIND DRIVEN BY SOLAR MAGNETOGRAMS

The model described above was tested for a nontilted, rotating magnetic dipole (with the field strength at the poles chosen as 3.87 G). We used this simple case to explore the consequences of the source terms we introduced in equations (1) and (2), as well as to filter out the right choice of parameters that produces the most realistic solar wind. The results of this comparison are shown in Figure 1. The solid curves in this figure correspond to simulation results, while the dotted curves represent *Ulysses* data obtained for the period from 1994 September through 1995 July. These data are normalized to 1 AU following Goldstein et

al. (1996). The set of parameters for this simulation run is as given above. As seen in the figure, the bimodal structure of the modeled solar wind is well reproduced. However, there is a lack of sharp transition between the two types of wind because of the insufficient numerical resolution.

Simulation results for a realistic magnetic field configuration at the Sun are shown in Figures 2, 3, and 4. To obtain the bulk solar magnetic fields, we followed the Potential Field Source Surface method by Altschuler et al. (1977). This method assumes that the magnetic field is a potential field and that the magnetic scalar potential is estimated as a series of spherical harmonics. The coefficients in the series[6] are chosen to fit *real* magnetogram data obtained from the Wilcox Solar Observatory. The source surface (where the scalar potential is equal to zero) is placed at radial distance $R_{ss} = 2.5\ R_\odot$ from the Sun. The function $\Lambda\,[B_R(\theta, \phi)]$ is chosen as $\{1 + (\Lambda_t - 1)\ \min\,[1, B_R(\theta, \phi)/B_0]\}$, where $B_0 = 3.87$ G as above. In this Letter, we present simulation results for Carrington rotation 1881 (with a central meridian on 1994 April 22). The left panel of Figure 2 shows a three-dimensional view of the field geometry near the Sun under steady state conditions. The sphere is placed at $R = R_\odot$, and the color code represents the solar wind speed. A three-dimensional view far from the Sun is shown in the right panel of Figure 2.

As seen in Figures 3 and 4, the fast wind (~790 km s^{-1}) correlates with open field regions, whereas the slow wind (~425 km s^{-1}) originates from helmet-type coronal streamers. The dense (~1.5×10^7 m^{-3}) and cool (~1.1×10^5 K) outflow is associated with closed field regions at the Sun, whereas in coronal holes we observe a rarefied (~5.0×10^6 m^{-3}; see the dashed contour line in black in Fig. 4) and hot (~3.1×10^5 K) solar wind. These results agree with the observed solar wind characteristics at 1 AU, both in a qualitative and a quantitative manner, despite the relatively course spatial resolution in our simulations (~3.438 $R_\odot$) at this radial distance from the Sun.

[6] They can be obtained from http://solar.stanford.edu/~wso/forms/prgs.html.

5. CONCLUSIONS

We used the concept of energy interchange between the plasma and turbulence, in terms of temperature relaxation, to describe the thermal properties of plasma and flow acceleration in the inner heliosphere. We developed an empirical model in which the low values of γ near the Sun are associated with the "turbulent" internal degrees of freedom; we allowed for γ to change with radial distance from the Sun, but a form of the total energy was conserved. By means of this approach, we were able to produce a steady state solar wind in simulations involving magnetic fields derived from observations, and we succeeded in obtaining results that are consistent with observed wind properties at 1 AU.

We believe that the computational techniques presented in this Letter open new doors to incorporating magnetic observations into numerical simulations aimed at modeling the global heliosphere and space weather. In a follow-up study, we intend to make a detailed comparison between MHD results and observational data, ranging from solar minimum to solar maximum conditions.

The authors thank T. G. Forbes, B. C. Low, T. Holzer, and an unknown referee for their comments. This research work was supported by DoD MURI grant F49620-01-1-0359, NSF CISE grant ACI-9876943, and NASA AISRP grant NAG5-9406 at the University of Michigan. G. Tóth acknowledges the support by OTKA grant T037548.

REFERENCES

Altschuler, M. D., Levine, R. H., Stix, M., & Harvey, J. 1977, Sol. Phys., 51, 345
Axford, W. I., & McKenzie, J. F. 1992, in Solar Wind Seven: Proc. Third COSPAR Colloq., ed. E. Marsch & R. Schwenn (Tarrytown: Pergamon), 1
Goldstein, B. E., et al. 1996, A&A, 316, 296
Groth, C. P. T., DeZeeuw, D. L., Gombosi, T. I., & Powell, K. G. 2000, J. Geophys. Res., 105, 25,053
Holzer, T. E., Flå, T., & Leer, E. 1983, ApJ, 275, 808
Linker, J. A., et al. 1999, J. Geophys. Res., 104, 9809
McKenzie, J. F., Axford, W. I., & Banaszkiewicz, M. 1997, Geophys. Res. Lett., 24, 2877
Phillips, J. L., et al. 1995, Geophys. Res. Lett., 22, 3301
Pneuman, G. W., & Kopp, R. A. 1971, Sol. Phys., 18, 258
Powell, K. G., Roe, P. L., Linde, T. J., Gombosi, T. I., & DeZeeuw, D. L. 1999, J. Comput. Phys., 154, 284
Riley, P., Linker, J. A., & Mikić, Z. 2001, J. Geophys. Res., 106, 15,889
Saurel, R., Chinnayya, A., & Renaud, F. 2003, Shock Waves, in press
Sokolov, I. V., Timofeev, E. V., Sakai, J. I., & Takayama, K. 2002, J. Comput. Phys., 181, 354
Steinolfson, R. S., & Hundhausen, A. J. 1988, J. Geophys. Res., 93, 14,269
Suess, S. T., Wang, A.-H., Wu, S. T., Poletto, G., & McComas, D. J. 1999, J. Geophys. Res., 104, 4697
Totten, T. L., Freeman, J. W., & Arya, S. 1995, J. Geophys. Res., 100, 13
Usmanov, A. V. 1993, Sol. Phys., 146, 377
Usmanov, A. V., Goldstein, M. L., Besser, B. P., & Fritzer, J. M. 2000, J. Geophys. Res., 105, 12,675
Wang, A.-H., Wu, S. T., Suess, S. T., & Poletto, G. 1998, J. Geophys. Res., 103, 1913
Wu, S. T., Guo, W. P., Michels, D. J., & Burlaga, L. F. 1999, J. Geophys. Res., 104, 14,789
Zeldovich, Ya. B., & Raizer, Yu. P. 2002, Physics of Shock Waves and High-Temperature Hydrodynamic Phenomena, ed. W. D. Hayes & R. F. Probstein (Mineola: Dover)